An Offset-Free Composite Model Predictive Control Strategy for DC/DC Buck Converter Feeding Constant Power Loads

Qianwen Xu, *Member, IEEE*, Yunda Yan, *Member, IEEE*, Chuanlin Zhang, *Senior Member, IEEE*, Tomislav Dragicevic, *Senior Member, IEEE*, and Frede Blaabjerg, *Fellow, IEEE*

***Abstract*—The high penetration of power electronic converters into dc microgrids may cause the constant power load stability issues, which could lead to large voltage oscillations or even system collapse. On the other hand, dynamic performance should be satisfied in the control of power electronic converter systems with small overshoot, less oscillations, and smooth transient performance. This article proposes an offset-free model predictive controller for a dc/dc buck converter feeding constant power loads with guaranteed dynamic performance and stability. First, a receding horizon optimization problem is formulated for optimal voltage tracking. To deal with the unknown load variation and system uncertainties, a higher order sliding mode observer is designed and integrated into the optimization problem. Then an explicit closed-loop solution is obtained by solving the receding horizon optimization problem offline. A rigorous stability analysis is performed to ensure the system large signal stability. The proposed controller achieves optimized transient dynamics and accurate tracking with simple implementation. The effectiveness of the proposed controller is validated by simulation and experimental results.**

***Index Terms*—Constant power load (CPL), large signal stability, model predictive control (MPC), nonlinear disturbance observer, offset-free tracking.**

I. Introduction

MICROGRIDS are building blocks for the future smart grids, which provide efficient integration of distributed sources [1]. Extensive research works have been conducted for ac microgrids due to their compatibility with conventional power systems. However, as most of the distributed sources are dc by nature (e.g., PV, fuel cell, energy storage systems, etc) and there are growing penetration of dc loads into the microgrids, dc microgrids provide increased efficiency and reliability with the reduction of power conversion stages [2], [3]. Moreover, dc microgrids are relatively simple to control compared to their ac counterparts, which have issues like synchronization, reactive power flow, and phase unbalance, etc. Therefore, dc microgrids have gained tremendous attention in recent years [4].

In dc microgrids, a great number of power electronic converters are installed as the interfaces for distributed sources and loads. They allow the controllability of sources and loads, and enable high conversion efficiency. However, the power electronic converters also bring the constant power load (CPL) issue: The power electronic converter loads, when tightly controlled, behave as CPLs with negative incremental impedance characteristics [5], [6]. The interaction of the CPLs with their respective source converters will decrease system damping and even cause instability issues [7], [8].

Many works have been conducted for stabilization of dc/dc converter systems with CPLs. Passive damping approaches can increase the system damping by adding necessary capacitors/resistors or designing proper *LC* filters [7], [9]. However, these methods are limited by physical constraints due to the increased weight/cost and power loss. Active damping methods are proposed to stabilize the system by modifying control loops to reshape load/source impedances [10]–[12]. However, these approaches utilize linearized small signal models and they can only ensure system stability around the operating points. When large signal disturbances happen, the system may be unstable.

Considering the nonlinearity of power electronic converters and the CPLs, several nonlinear approaches have been proposed to stabilize CPLs in a large signal sense. A boundary controller is proposed for stabilizing buck converter to overcome the destabilizing effects introduced by CPLs even in the presence of unknown parameters [13]. But the controller is designed on a hysteresis band, which results in variable switching frequency and degraded ripple effect. In [14], a sliding mode duty ratio controller for a buck converter at a fixed switching frequency is proposed and it can stabilize the CPLs over a wide operating range. However, it requires the measurement of dc capacitor

Manuscript received April 23, 2019; revised July 27, 2019; accepted September 11, 2019. Date of publication September 15, 2019; date of current version February 11, 2020. This work was supported in part by Wallenberg-NTU Presidential Postdoc Fellowship in Nanyang Technological University, Singapore, in part by the Reliable Power Electronic-Based Power System (REPEPS) project at the Department of Energy Technology, Aalborg University as a part of the Villum Investigator Program funded by the Villum Foundation, in part by the Program for Professor of Special Appointment (Eastern Scholar) at Shanghai Institutions of Higher Learning, and in part by the Natural Science Foundation of Shanghai under Grant 19ZR1420500. Recommended for publication by Associate Editor T. Suntio. *(Corresponding author: Chuanlin Zhang.)*

Q. Xu is with the School of Electrical and Electronic Engineering, Nanyang Technological University, Singapore (e-mail: qianwen.xu@ntu.edu.sg).

Y. Yan is with the Key Laboratory of Measurement and Control of CSE, Ministry of Education, School of Automation, Southeast University, Nanjing 210096, China (e-mail: yd.yan@ieee.org).

C. Zhang is with the Intelligent Autonomous Systems Lab, College of Automation Engineering, Shanghai University of Electric Power, Shanghai 200090, China (e-mail: clzhang@shiep.edu.cn).

T. Dragicevic and F. Blaabjerg are with the Department of Energy Technology, Aalborg University, 9100 Aalborg, Denmark (e-mail: tdr@et.aau.dk; fbl@et.aau.dk).

Color versions of one or more of the figures in this article are available online at http://ieeexplore.ieee.org.

Digital Object Identifier 10.1109/TPEL.2019.2941714

current, leading to a high equivalent series resistance and degraded ripple filtering effect. In [15], a composite nonlinear controller is proposed for stabilizing dc/dc boost converter, where a nonlinear disturbance observer is designed for accurate tracking and a backstepping controller is designed for large signal stabilization. An adaptive backstepping (AB) controller is proposed in [16] for stabilizing boost converter feeding CPLs with a third degree cubature Kalman filter (CKF) for uncertainty estimation. An estimation-based robust feedback controller with third degree CKF estimator is proposed for stabilizing CPLs in [17]. In [18], an adaptive passivity-based controller for dc/dc buck converter feeding CPLs, where a nonlinear disturbance observer is designed to improve the control robustness and the passivity-based control guarantees large signal stability. However, for all these nonlinear control methods, the optimal performance with smooth transients (e.g., small overshoot, less oscillations, and small settling time) cannot easily be achieved.

As a powerful technique for optimized performance tracking, model predictive control (MPC) has attracted great attention in power converters and electrical drives [19]–[22]. MPC obtains control signal by solving an optimization problem with future behavior over a time horizon with the system nonlinearties taken into consideration. However, in these MPC works [19]–[21], accurate system model is required to achieve high-precision tracking performance, which is always hindered by system uncertainties and external disturbances in real situations. Combining MPC with disturbance observation/compensation process is a possible solution. A continuous MPC controller integrating with a nonlinear disturbance observer is proposed for a buck converter aiming to realize accurate voltage tracking [22]. However, it only considers resistive load and the CPL is not included, which brings the nonlinearity and negative impedance instability issue.

In this article, a novel offset-free composite MPC is proposed for stabilizing dc/dc buck converter feeding CPLs. First, a receding horizon optimization problem is formulated for optimal voltage tracking and the future tracking error is predicted by Taylor series expansion. To deal with unknown external and model uncertainties, a higher order sliding mode observer (HOSMO) is designed to estimate the future tracking error. The HOSMO technique is selected as it enables a finite-time convergence rate of disturbance identification processes [23], [24]. Combined with the HOSMO, an explicit closed-loop solution is obtained by solving the estimated receding-horizon optimization problem. A rigorous stability analysis is conducted to ensure stability of the closed-loop system under the proposed controller. Compared with existing related works, the main contributions of this article include:

1) Offset-free voltage tracking: With the integrated HOSMO in the MPC optimization problem, the proposed controller achieves offset-free tracking with robustness against the unknown external and model uncertainties.
2) Large signal stability: With a rigorous stability analysis of the closed-loop system under the proposed offset-free MPC controller, system large signal stability is assured.
3) Optimal design with simple implementation: The optimal design parameters are directly obtained from the explicit MPC solution, which could guarantee optimized system transient performance (e.g., small overshoot, smooth transition, and less oscillations).

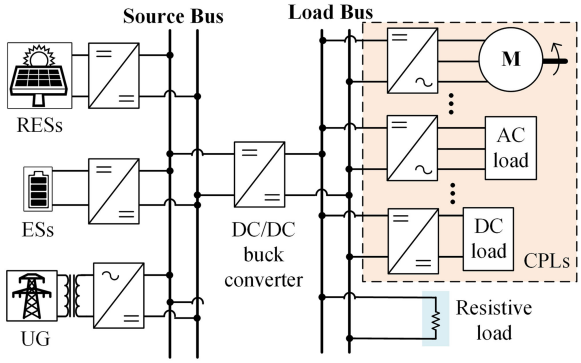

Fig. 1. General structure of a dc microgrid with power electronics-based generators and loads.

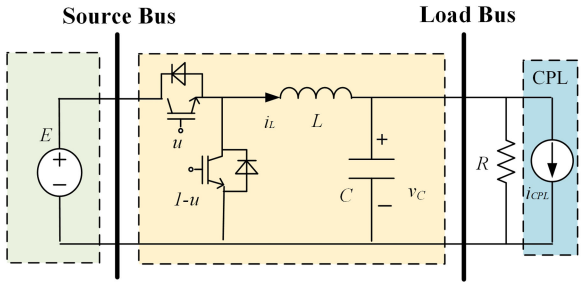

Fig. 2. Buck converter feeding CPLs.

The rest of this article is organized as follows: Section II presents the system under study and the problem formulation. The proposed offset-free MPC controller is illustrated in Section III. Section IV and Section V demonstrate the simulation and experimental verification studies, respectively. The conclusions are drawn in Section VI.

II. System Modeling and Problem Description

Fig. 1 shows a general structure of a dc microgrid [18]. The source bus is supplied by the renewable resources, energy storage systems, and the main ac grid (if it is grid connected). The dc/dc buck converter is used to step down the bus voltage for load voltage levels. This type of architecture can be found in numerously types of systems, including data center and telecom power supply systems, electrical vehicles, ships, and electric aircrafts. The loads include dc/dc converter load, dc/ac inverter load, dc/ac inverter fed motor drive load, and resistive load. The first three loads are tightly regulated converter loads, known as CPLs. They can all be lumped and modeled as

$$i_{\mathrm{CPL}} = \frac{P_{\mathrm{CPL}}}{v_C}. \tag{1}$$

The system in Fig. 1 can be simplified as a buck converter feeding a CPL with the power of P_{CPL} and a resistive load with the resistor of R, as is depicted in Fig. 2. Its dynamic model is represented by

$$\begin{cases} C\frac{dv_C}{dt} = i_L - \frac{v_C}{R} - \frac{P_{\mathrm{CPL}}}{v_C} \\ L\frac{di_L}{dt} = Eu - v_C \end{cases} \tag{2}$$

where i_L and v_C are the instantaneous inductor current and capacitor voltage of buck converter; E is the voltage of the source bus; L and C are the inductance and capacitance values; u is the duty ratio of the switch, which is the control signal to be designed. As can be observed in (2), there is a nonlinear term $\frac{P_{\rm CPL}}{v_C}$.

Considering the model uncertainties and load variations, the dynamic model in (2) is further expressed as

$$\begin{cases} C_0 \frac{dv_C}{dt} = i_L + d_1 \\ L_0 \frac{di_L}{dt} = E_0 u - v_C + d_2 \end{cases} \tag{3}$$

where L_0, C_0, and E_0 are the nominal values of inductance, capacitance, and source bus voltage; d_1 and d_2 are lumped uncertainties, denoted by

$$d_1 = -\frac{v_C}{R} - \frac{P_{\rm CPL}}{v_C} - \Delta C \frac{dv_C}{dt} \tag{4}$$

$$d_2 = \Delta E u - \Delta L \frac{di_L}{dt} \tag{5}$$

where ΔL, ΔC, and ΔE are the uncertain variations of inductance, capacitance, and source voltage to their respective nominal values.

The objective of the buck converter system is to track its bus voltage reference accurately with optimal transient performance even under large load variations and system uncertainties.

III. Proposed Controller

This section presents the design procedure of the proposed offset-free MPC controller. The objective of the proposed controller is to solve the optimal tracking problem of the buck converter system so that the output voltage tracks its reference value with the guaranteed dynamic performance, robustness, and stability.

To make the derivations more readable, the functions of some symbols are declared here first: The r-th order derivatives of variables are denoted by $(\bullet)^{(\rm r)}$, the estimates of the variables are denoted by the hatted symbol ($\hat{\bullet}$), and the predictions of the variables within a receding horizon time interval are denoted by the barred symbol ($\bar{\bullet}$).

A. Model Prediction

According to the nominal MPC theory, the cost function for the buck converter can be defined as

$$J(t) \triangleq \frac{1}{2} \int_0^T Q(V_{\rm ref}(t+\tau) - v_C(t+\tau))^2 + R(u_r(t+\tau) - u(t+\tau))^2 d\tau \tag{6}$$

where the first term describes the voltage tracking error, which is to make the output voltage v_C accurately track its reference voltage $V_{\rm ref}$; the second term describes the control input deviation error, which provides additional freedom to penalize the control energy and admits the integral control optimization. $u_r(t)$ is the desired steady-state, which will be estimated by the HOSMO later. $T > 0$ is the predictive period; $Q > 0$ and $R \geq 0$ are weighting gains on the tracking error and control input error, respectively.

To start with, the following transformation is defined to construct the optimal tracking problem of the system in (3) with one order control taken into consideration:

$$\begin{cases} e(t) \triangleq V_{\rm ref} - v_C \\ e_1(t) \triangleq \dot{e}(t) = -\frac{1}{C_0}(i_L + d_1) \\ e_2(t) \triangleq \dot{e}_1(t) = -\frac{E_0}{L_0 C_0} u + \frac{v_C}{L_0 C_0} - \frac{d_2}{L_0 C_0} - \frac{d_1^{(1)}}{C_0} \\ e_3(t) \triangleq \dot{e}_2(t) = -\frac{E_0}{L_0 C_0} u^{(1)} + \frac{v_C{}^{(1)}}{L_0 C_0} - \frac{d_2{}^{(1)}}{L_0 C_0} - \frac{d_1^{(2)}}{C_0} \end{cases} \tag{7}$$

where $u^{(1)}(t)$ represents the derivative of $u(t)$.

By defining $b_0 = \frac{E_0}{L_0 C_0}$, $w_n(t) = \frac{v_C}{L_0 C_0}$, $w(t) = -\frac{d_2}{L_0 C_0} - \frac{d_1^{(1)}}{C_0}$ in (7), the tracking dynamics of $e_2(t)$ and $e_3(t)$ can be further expressed as

$$\begin{cases} e_2(t) = -b_0 u + w_n(t) + w(t) \\ e_3(t) = -b_0 u^{(1)} + w_n^{(1)}(t) + w^{(1)}(t) \end{cases} \tag{8}$$

where uncertainties are included in functions $w(t)$ and $w^{(1)}(t)$.

Using Taylor series expansion, the future tracking error within the predictive period is expressed as

$$e(t+\tau) = e(t) + \tau e_1(t) + \frac{\tau^2}{2} e_2(t) + \frac{\tau^3}{6} e_3(t). \tag{9}$$

The values can be estimated by observers, which will be discussed in the next section. With estimated values, the predicted tracking error is presented as

$$\bar{e}(t+\tau) = e(t) + \tau \hat{e}_1(t) + \frac{\tau^2}{2} \hat{e}_2(t) + \frac{\tau^3}{6} \hat{e}_3(t). \tag{10}$$

The predicted tracking error in (10) can be written in the compact form as

$$\bar{e}(t+\tau) = \begin{bmatrix} \bar{\Gamma}(\tau) & \tilde{\Gamma}(\tau) \end{bmatrix} \begin{bmatrix} \bar{\varepsilon}(t) \\ \tilde{\varepsilon}(t) \end{bmatrix} \tag{11}$$

where $\bar{\Gamma}(\tau) \triangleq [\,1 \;\; \tau\,]$, $\tilde{\Gamma}(\tau) \triangleq [\,\frac{\tau^2}{2} \;\; \frac{\tau^3}{6}\,]$, $\bar{\varepsilon}(t) \triangleq [\,e(t) \;\; \hat{e}_1(t)\,]^\top$, $\tilde{\varepsilon}(t) \triangleq [\,\hat{e}_2(t) \;\; \hat{e}_3(t)\,]^\top = -b_0 U(t) + W_n(t) + W(t)$, $U(t) \triangleq [\,u(t) \;\; u^{(1)}(t)\,]^\top$, $W_n(t) \triangleq [\,w_n(t) \;\; w_n^{(1)}(t)\,]^\top$ and $W(t) \triangleq [\,w(t) \;\; w^{(1)}(t)\,]^\top$.

The future control input and desired future control signal are obtained as

$$\bar{u}(t+\tau) = \bar{\Gamma}(\tau) U(t) \tag{12}$$

$$\bar{u}_r(t+\tau) = \frac{1}{b_0} \bar{\Gamma}(\tau) \left[W_n(t) + W(t) \right]. \tag{13}$$

B. Design of Observer

In order to obtain the estimation values $\hat{e}_1$ and $\hat{w}$ in (10) and (13), the HOSMO technique is applied, which presents higher precision than other observation techniques [24]. The design of HOSMO is briefly introduced in Appendix A.

According to (4), (5), (7), and (8), $e_1(t)$ and $w(t)$ are bounded due to their relationship with physical electrical variables. Then the prerequisite of designing a HOSMO for estimating $e_1(t)$ and $w(t)$ is satisfied. By following [25] and Appendix A, a HOSMO

is designed as

$$\begin{cases} \dot{\hat{e}}(t) = \hat{e}_1(t) + v_0(t) \\ \dot{\hat{e}}_1(t) = -b_0 u^*(t) + w_n(t) + \hat{w}(t) + v_1(t) \\ \dot{\hat{w}}(t) = v_2(t) \\ v_0(t) = -\lambda_0 L_d^{\frac{1}{3}} |\hat{e}(t) - e(t)|^{\frac{2}{3}} \text{sign}(\hat{e}(t) - e(t)) \\ v_1(t) = \lambda_1 L_d^{\frac{1}{2}} |v_0(t)|^{\frac{1}{2}} \text{sign}(v_0(t)) \\ v_2(t) = \lambda_2 L_d \text{sign}(v_1(t)) \end{cases} \tag{14}$$

where L_d is a known positive constant with $L_d \geq |w(t)|$; $\lambda_i > 0, i = 0, 1, 2$ are tunable observer gains.

The error dynamics of the HOSMO system in (14) can be obtained as

$$\begin{cases} \dot{\sigma}_0 = -\lambda_0 L_d^{\frac{1}{3}} |\sigma_0|^{\frac{2}{3}} \text{sign}(\sigma_0) + \sigma_1 \\ \dot{\sigma}_1 = -\lambda_1 L_d^{\frac{1}{2}} |\sigma_0|^{\frac{1}{2}} \text{sign}(\sigma_1 - \dot{\sigma}_0) + \sigma_2 \\ \dot{\sigma}_2 \in -\lambda_2 L_d \text{sign}(\sigma_2 - \dot{\sigma}_1) + [-L_d, L_d] \end{cases} \tag{15}$$

where $\sigma_i \triangleq \hat{e}_i(t) - e_i(t), i = 0, 1$ and $\sigma_2 \triangleq \hat{w}(t) - w(t)$.

As proved in [25], the estimation error system (15) is finite-time stable, i.e., there exists a finite time constant $0 < t_f < \infty$ such that $\sigma_i (i = 0, 1, 2)$ are bounded if $0 \leq t < t_f$, and $\sigma_i \equiv 0$ if $t \geq t_f$. Then the finite-time convergences of the estimated values $\hat{e}_1$ and $\hat{w}$ in HOSMO (14) to their respective real values $e_1(t)$ and $w(t)$ are achieved.

C. Design of Optimal Control Law

By substituting (11)–(13) into (6), the performance index in (6) is estimated as

$$\begin{aligned} \bar{J}(t) \triangleq & \frac{1}{2} \int_0^T Q\bar{e}(t+\tau)^\top \bar{e}(t+\tau) + R(\bar{u}(t+\tau) \\ & - \bar{u}_r(t+\tau))^\top (\bar{u}(t+\tau) - \bar{u}_r(t+\tau)) d\tau \\ = & \frac{1}{2} Q\bar{\varepsilon}^\top \Gamma_1 \bar{\varepsilon} - b_0 Q\bar{\varepsilon}^\top \Gamma_2 \left(U(t) - \frac{W_n(t) + W(t)}{b_0} \right) \\ & + \frac{1}{2} \left(U(t) - \frac{W_n(t) + W(t)}{b_0} \right)^\top (b_0^2 Q\Gamma_3 + R\Gamma_4) \\ & \times \left(U(t) - \frac{W_n(t) + W(t)}{b_0} \right) \end{aligned} \tag{16}$$

where Γ_1, Γ_2, and Γ_3 are defined and calculated as

$$\Gamma_1 \triangleq \int_0^T \bar{\Gamma}^\top \bar{\Gamma} d\tau = \begin{bmatrix} T & \frac{T^2}{2} \\ \frac{T^2}{2} & \frac{T^3}{3} \end{bmatrix}$$

$$\Gamma_2 \triangleq \int_0^T \bar{\Gamma}^\top \tilde{\Gamma} d\tau = \begin{bmatrix} \frac{T^3}{6} & \frac{T^4}{24} \\ \frac{T^4}{8} & \frac{T^5}{30} \end{bmatrix}$$

$$\Gamma_3 \triangleq \int_0^T \tilde{\Gamma}^\top \tilde{\Gamma} d\tau = \begin{bmatrix} \frac{T^5}{20} & \frac{T^5}{72} \\ \frac{T^6}{72} & \frac{T^6}{252} \end{bmatrix}.$$

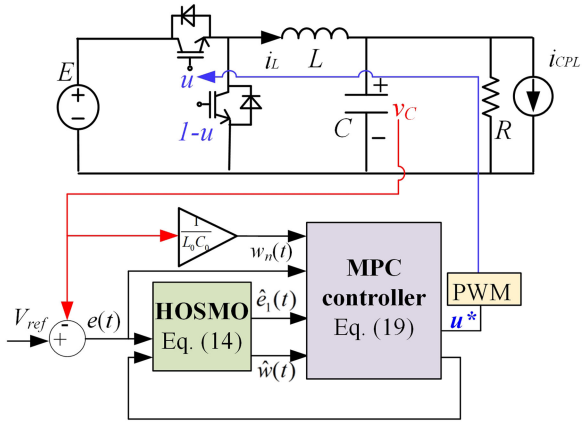

Fig. 3. Control diagram of the proposed offset-free MPC controller.

To get the optimal control law of $u(t)$, the partial derivative of $\bar{J}$ with respective to $U(t)$ is taken as

$$\begin{aligned} \frac{\partial \bar{J}}{\partial u} = & -b_0 Q\bar{\varepsilon}^\top \Gamma_2 \\ & + (b_0^2 Q\Gamma_3 + R\Gamma_1) \left(U(t) - \frac{W_n(t) + W(t)}{b_0} \right). \end{aligned} \tag{17}$$

Letting $\frac{\partial \bar{J}}{\partial U} = 0$ and $\frac{\partial^2 \bar{J}}{\partial U^2} > 0$, the optimal control law is obtained as

$$U^*(t) = \frac{1}{b_0} \left(\left(\Gamma_3 + \frac{1}{b_0^2} \frac{R}{Q} \Gamma_1 \right)^{-1} \Gamma_2^\top \bar{\varepsilon} + W_n(t) + W(t) \right). \tag{18}$$

Recalling that $\tilde{\varepsilon}(t) = [e(t)\ \hat{e}_1(t)]^\top, U(t) = [u(t)\ u^{(1)}(t)]^\top$, $W_n(t) = [w_n(t)\ w_n^{(1)}(t)]^\top$ and $W(t) = [w(t)\ w^{(1)}(t)]^\top$, and solving (18), the optimal control law u(t) can be derived as

$$u^*(t) = \frac{1}{b_0} (k_0 e + k_1 \hat{e}_1 + w_n + \hat{w}) \tag{19}$$

where $[k_0\ k_1]$ are designed as the first row values of $(\Gamma_3 + \frac{1}{b_0^2} \frac{R}{Q} \Gamma_1)^{-1} \Gamma_2^\top$, expressed as

$$\begin{cases} k_0 = (15T^6 + 6300T^2 h)/(T^8 + 1224T^4 h + 15120h^2) \\ k_1 = (6T^7 + 4536T^3 h)/(T^8 + 1224T^4 h + 15120h^2) \end{cases} \tag{20}$$

where $h \triangleq \frac{1}{b_0^2} \frac{R}{Q}$.

Therefore, the proposed MPC controller is designed by combining (7), (14), (19), and (20). The control diagram of the proposed approach is presented in Fig. 3.

D. Stability Analysis

To show the large signal stability of the proposed approach, a rigorous stability analysis is presented here.

Theorem: The closed-loop system (3), (7), (14), and (19) is asymptotically stable.

Proof: Designed from (20), it is obvious that k_0 and k_1 are positive values. If there is no disturbance, $p(s) = s^2 + k_1 s + k_0$

is Hurwitz and thus the system (3), (7), and (19) is asymptotically stable.

With the presence of disturbances, the closed-loop system (3), (7), (14), and (19) can be written as

$$e_2(t) + k_1 e_1(t) + k_0 e(t) + g(t) = 0 \tag{21}$$

where $g(t) \triangleq k_1\sigma_1 + \sigma_2$ according to the error dynamics of HOSMO in (15); $|g(t)| \le \gamma$ ($\gamma \ge 0$) for $0 \le t < t_f$, and $g(t) \equiv 0$ for $t \ge t_f$.

Rewrite the system in (21) in the following compact form:

$$\dot{\varepsilon}(t) = A\varepsilon(t) + Bg(t) \tag{22}$$

where $\varepsilon(t) \triangleq [e(t)\ e_1(t)]^\top$, $A \triangleq \begin{bmatrix} 0 & 1 \\ -k_0 & -k_1 \end{bmatrix}$ and $B \triangleq [0\ -1]^\top$.

Based on linear control theory [26], the solution of (22) can be expressed as

$$\varepsilon(t) = \exp(At)\varepsilon(0) + \int_0^t \exp(A(t-\tau))Bg(\tau)d\tau. \tag{23}$$

The following inequality relationship holds for (23):

$$\|\varepsilon(t)\| \le \|\exp(At)\| \cdot \|\varepsilon(0)\| + \gamma \int_0^t \|\exp(A(t-\tau))\| d\tau. \tag{24}$$

Based on Lemma 1 in Appendix, (24) can be further developed as

$$\|\varepsilon(t)\| \le \delta t^2 \exp(\alpha(A)t)\,\|\varepsilon(0)\| + \frac{\delta\gamma}{\alpha(A)^3}((\alpha(A)^2 t^2 - 2\alpha(A)t + 2)\exp(\alpha(A)t) - 2) \tag{25}$$

where $\delta \triangleq \sum_{k=0}^{1} \|N\|^2/k! \ge 0$ and N is the Schur decomposition matrix of A.

As can be observed from (25), within any finite time ($0 \le t < t_f$), $\varepsilon(t)$ is bounded. When $t \ge t_f$, the system is reduced to $\dot{\varepsilon}(t) = A\varepsilon(t)$ with the characteristics equation $p(s) = s^2 + k_1 s + k_0$. Therefore, the parameters designed from (20) can ensure the asymptotic stability of system. ■

IV. Simulation Results

The system model in Fig. 2 with the proposed controller in Fig. 3 is tested in MATLAB/Simulink to verify its effectiveness in terms of large signal stability, optimized dynamics, and accurate tracking against uncertainties. System parameters are listed in Table I.

TABLE I
System Parameters and Control Parameters

Variables	Description	Value
V_{ref}	Load bus voltage reference	100 V
f_s	Switching frequency	20 kHz
Q	Weighting gain of tracking error	1
E_0	Nominal converter input voltage	200 V
L_0	Nominal inductance	2 mH
C_0	Nominal capacitance	1 mF
L_d	HOSMO constant	10^{15}
$\lambda_0, \lambda_1, \lambda_2$	HOSMO gains	4,3,2

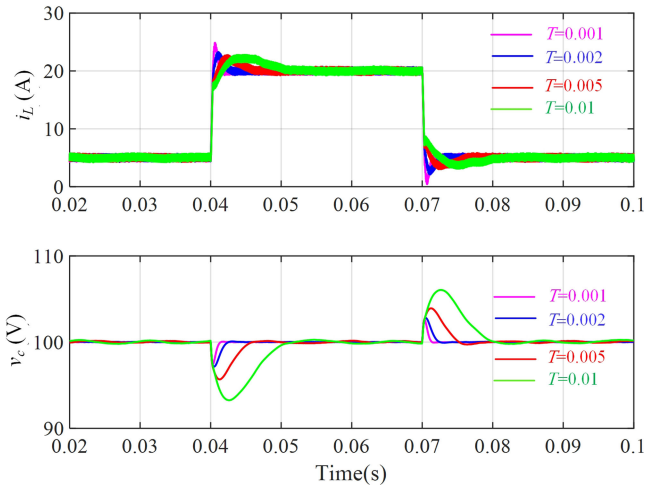

Fig. 4. System dynamic response with different values of predictive period T.

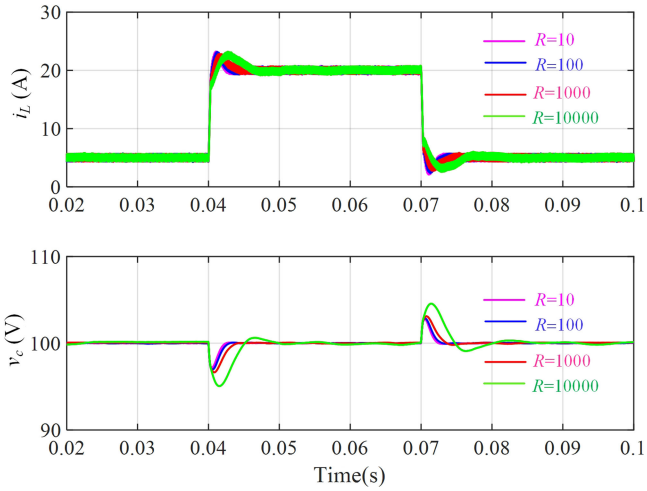

Fig. 5. System dynamic response with different values of control input signal weighting gain R.

A. Parameter Selection

According to (19), the design of the proposed MPC controller requires the selection of the predictive period T and the ratio of weighting gains R/Q. For simplicity, weighting gain Q is set at 1 and R is to be selected.

Fig. 4 shows system dynamic response with different values of predictive period T ($T = 0.001, 0.002, 0.005$, and 0.01). The weighting gain R is to mitigate the control variation, thus its impact is smaller and it can be set at zero first for selecting T. The CPL steps up from 500 W to 2 kW at 0.04 s and steps back to 500 W at 0.07 s. It can be observed that, with the load variation, bus voltage can track the reference value accurately with smooth transients and the settling time is around the predictive period T. Therefore, by choosing T as the required settling time, offset-free tracking with optimal transient can be obtained.

Fig. 5 shows system dynamic response with different values of weighting gain R (R = 10, 100, 1000, and 10 000).

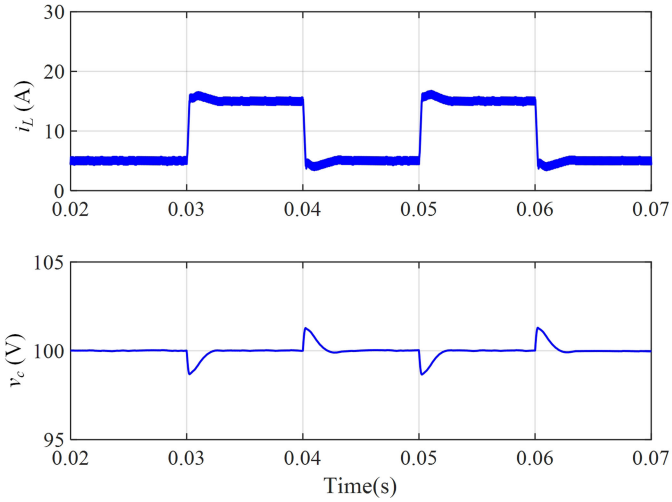

Fig. 6. Simulation results of the proposed controller with the variation of CPL and resistive load.

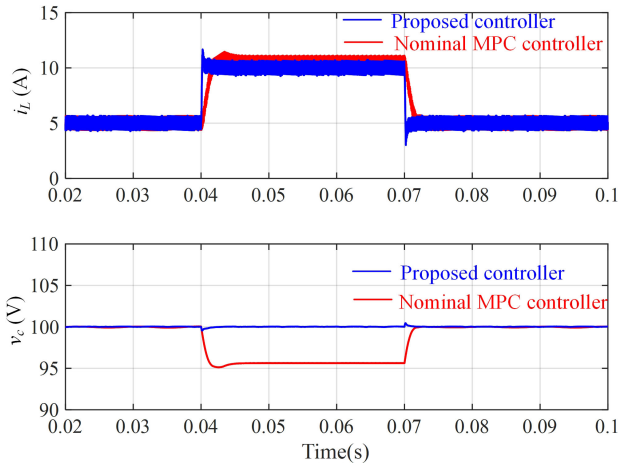

Fig. 7. Simulation results with the variation of CPL for the proposed controller and nominal MPC controller.

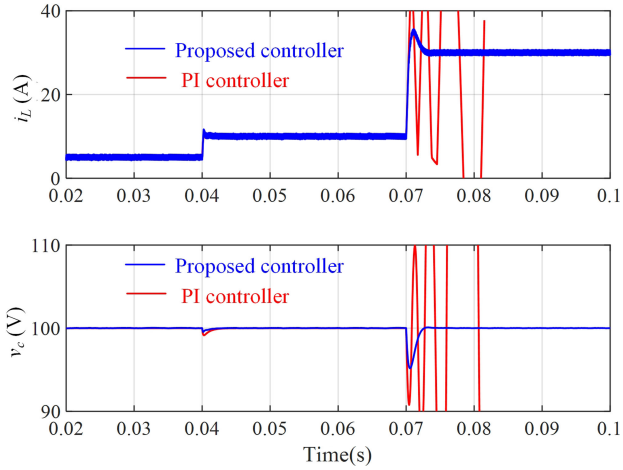

Fig. 8. Simulation results with the variation of CPL for the proposed controller and double-loop PI controller.

The predictive period T is fixed at 0.002. It reveals that a larger R will cause a slower response and may cause small deviations. But there is a tradeoff that smaller R will lead to larger control energy.

Therefore, given the desired dynamic performance, T and R can be selected to achieve optimal transient performance. Here T is selected as 0.002 and R is selected as 10 for the later case studies.

B. Simulation Verification

The simulation results of the proposed controller with the variation of CPL and resistive load are presented in Fig. 6. Initially, 500 W CPL is connected to the bus and there is no resistive load; then 1 kW resistive load is connected at 0.03 s and disconnected at 0.04 s; at 0.05 s, CPL increases from 500 to 1500 W; at 0.06 s, CPL steps back to 500 W. As can be observed, the smooth transient performance is achieved with the settling time around 2 ms and maximum transient voltage deviation less than 1% with three times load variation; after transients, load bus voltage is regulated accurately at the reference value 100 V. It reveals that the proposed controller achieves smooth transients with accurate tracking for the integration of both resistive load and CPL.

As the worst case in terms of stability is the pure CPL case, in this regard, only CPL is connected to the load bus in the following studies.

To show the advantage of the proposed controller compared with a nominal MPC controller without observers, simulations are conducted and the results are presented in Fig. 7. The design of the nominal MPC controller is the same as the proposed controller except that the HOSMO is eliminated and e_1 is calculated based on the nominal power 500 W and nominal input voltage 200 V. As can be observed in Fig. 7, with the CPL variation from 500 to 1000 W and 1000 to 500 W, the output voltage cannot accurately track at the reference value and there is a large deviation value of 4.5 V from the reference value 100 V. But for the proposed controller, accurate voltage tracking is achieved. This shows the advantage of the proposed controller in offset-free voltage tracking.

To verify the large signal stability of the proposed controller, a comparison is made between the proposed controller and the conventional double-loop PI controller, as is shown in Fig. 8. It is known that PI controllers have tradeoff in stability margin and dynamic response speed, i.e., faster dynamics will lead to less stability margin [27]. To have a fair comparison, the parameters for the PI controller are well-tuned with the voltage control bandwidth at 500 Hz and current control bandwidth at 5000 Hz so that the system under the PI controller can achieve similar dynamics of that under the proposed controller. The parameter design procedure of the double-loop PI controller is briefly illustrated in Appendix D. Step changes of CPL are performed for both controllers. At 0.04 s, CPL increases from 500 W to 1 kW. It shows that both systems are stable with similar settling time (2 ms) and the proposed controller even has smaller voltage dip during transient compared with PI controller. At 0.07 s, when

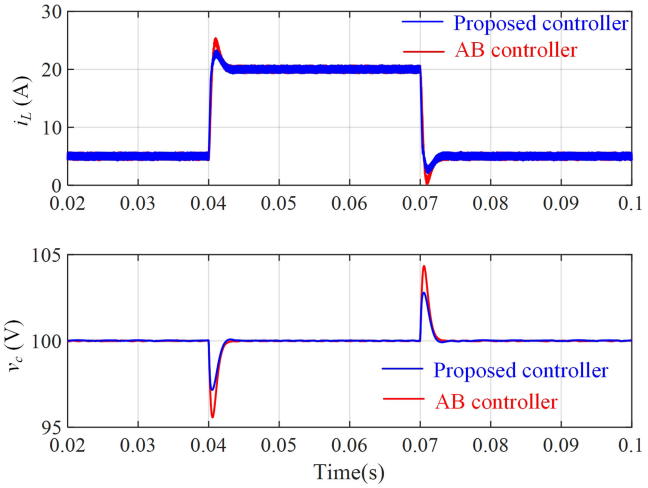

Fig. 9. Simulation results with the variation of CPL for the proposed controller and AB controller [15].

CPL increases from 1 to 3 kW, the system under PI controller becomes unstable while the system under the proposed controller still maintains stable with smooth dynamics. Therefore, with similar dynamic performance, the proposed controller can guarantee smooth and accurate voltage tracking with stable operation under large CPL variation, whereas the conventional PI controller fails to do so. This verifies the advantage of the proposed controller in terms of large signal stability.

To show the superiority of the proposed controller in achieving optimized transient performance (e.g., small deviation and smooth transition), the proposed controller is compared with AB controller in [15], as presented in Fig. 9. The AB controller is a nonlinear controller that can stabilize CPLs with fast dynamics and accurate tracking [15]. At 0.04 s, CPL steps up from 500 W to 2 kW and at 0.07 s CPL steps back to 500 W. As can be observed, both controllers can stabilize CPLs with fast dynamics and accurate tracking, while the proposed controller achieves smaller voltage dip and smaller current overshoot.

Fig. 10 shows the impact of the input voltage variation under the proposed controller. The load maintains at 1 kW. The source bus voltage E varies from 200 to 400 V at 0.04 s and 400 to 200 V at 0.07 s. As can be observed, with the step variations of source bus voltage, the load bus voltage is regulated accurately at 100 V in optimized dynamics within 2 ms. The inductor current is negligibly affected. Thus the system ensures stable operation under the variation of source bus voltage.

To demonstrate the robustness of the proposed controller against model uncertainties, simulation studies with different uncertain inductance values and capacitance values are investigated. Fig. 11 shows the system dynamic performance with different deviation values of inductance ΔL at -20%, 0, 20%, and 40%. The real inductance value L is $L_0(1+\Delta L)$. For all the cases, with load step variations, system bus voltage accurately tracks the reference value at 100 V within fast transient (less than 2 ms) and small transient deviation. Thus the uncertainties in inductance value will not impact system performance under the proposed controller. Similarly, Fig. 12 presents the system

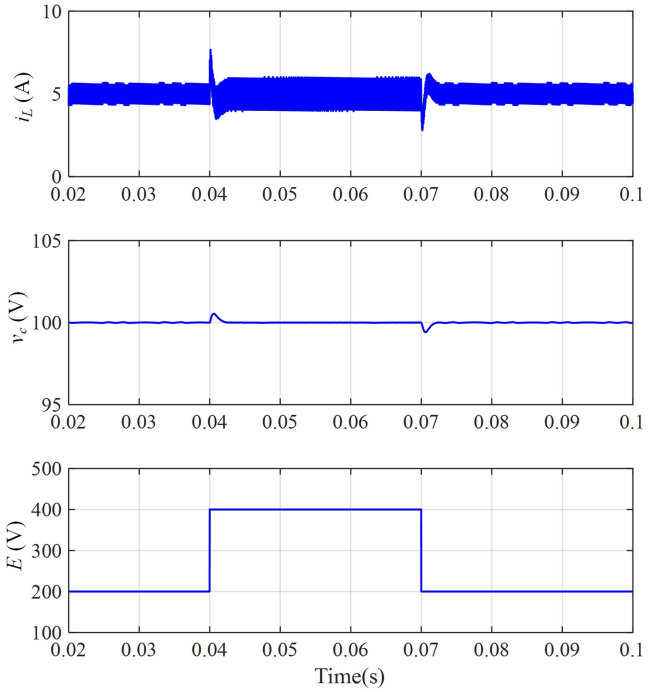

Fig. 10. Simulation results with the variation of source side voltage.

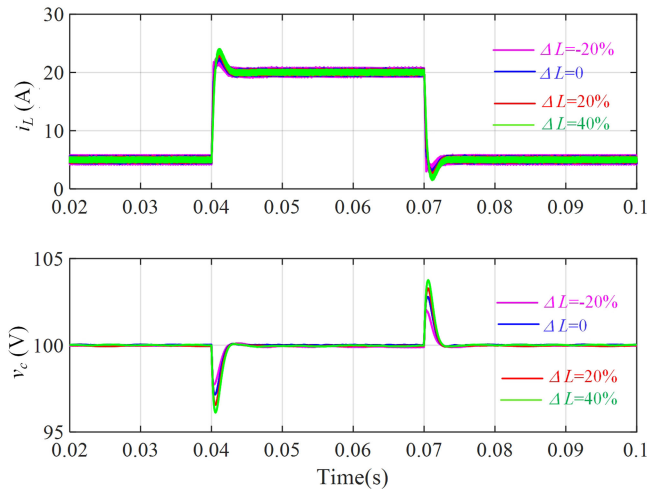

Fig. 11. Simulation results with the uncertain inductance values.

dynamics with different deviation values of capacitance ΔC at -20%, 0, 20%, and 40%. The real capacitance value C is $C_0(1+\Delta C)$. Simulation results illustrate that output voltage always tracks the reference value accurately with different deviation values of capacitance to its nominal value. Therefore, it is concluded that the proposed controller achieves offset-free tracking with robustness against the model uncertainties.

C. Discussions

The advantages of the proposed controller include the offset-free voltage tracking, large signal stabilization, optimized performance, and strong robustness against uncertainties. Compared with a nominal MPC controller, the integration of

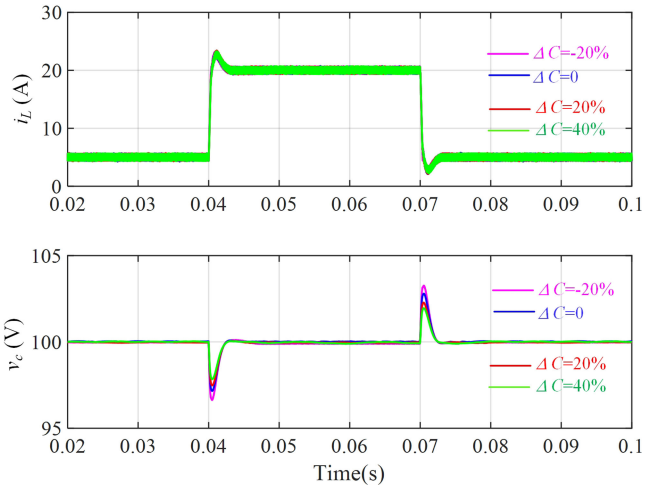

Fig. 12. Simulation results with the uncertain capacitance values.

the HOSMO makes the proposed controller achieve offset-free and accurate voltage tracking, as illustrated in Fig. 7; compared with linear PID controller, the proposed controller achieves large signal stability under large signal disturbances, as illustrated in Fig. 8; compared with other nonlinear controller (e.g., AB), it provides optimized performance with smooth transients (e.g., small overshoot, less oscillations, and small settling time), as illustrated in Fig. 9. It has strong robustness against uncertainties, as demonstrated by Figs. 10 and 11 with the variations of input voltage, inductance value, and capacitance value, respectively.

The proposed controller might have some limitations. First, for the parameter tuning of the proposed method, it is based on empirical experience with trial and error until we reach the expected dynamic performance, like existing nonlinear methods. But once the parameters T and R are settled, the control gains k_0 and k_1 are optimally obtained to achieve the optimized performance. And the procedure for tuning T and R can follow the presentation in Section IV. A with simulation results in Figs. 4 and 5.

In addition, because the proposed method is a totally new method for stabilizing power electronic converter systems with optimized performance, to the current stage, we only apply this method in buck converter systems. For the boost converter or buck/boost converter, because their models are bilinear, transformations are required and there will be some differences in designing cost functions. In our future works, we will extend this method to other converter topologies to make it a more general approach.

V. Experimental Results

To further verify the effectiveness of the proposed controller, an experimental setup of a buck converter system is built in the laboratory, as shown in Fig. 13. It consists of a dc power source, a dc/dc buck converter, dSPACE DS1006, and a programmable load. The proposed control algorithm in Fig. 3 is implemented in dSPACE to generate PWM signals for the dc/dc buck converter.

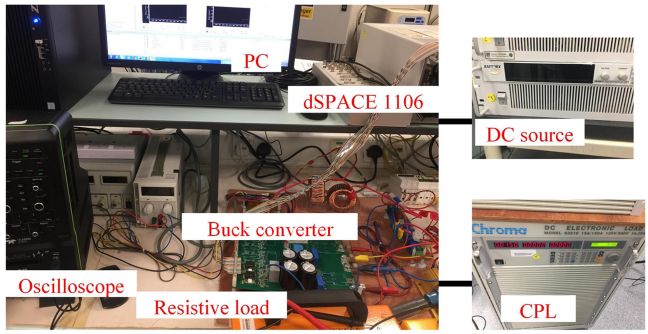

Fig. 13. Experimental setup.

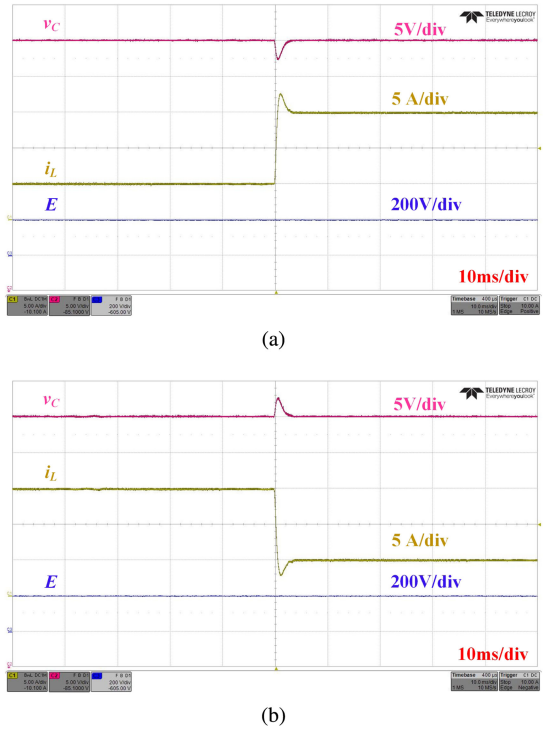

Fig. 14. Experimental results with CPL variation.

System and control parameters are the same as that listed in Table I and in simulation studies. Chroma programmable load is configured to operate in constant power mode to emulate the CPL.

Fig. 14 shows experimental results with the proposed controller with the variation of CPL. Fig. 14(a) presents the dynamic response when CPL steps up from 500 to 1500 W; Fig. 14(b) presents the dynamic response when CPL steps down from 1500 to 500 W. It is shown that at each step variation, the bus voltage responds immediately and tracks the reference value accurately within a settling time less than 2 ms. Stable operation is achieved with smooth transient performance.

Experimental results of input voltage, bus voltage, and inductor current are presented in Fig. 15 to illustrate the proposed controller with the input voltage variation. Fig. 15(a) shows system performance when the input voltage increases

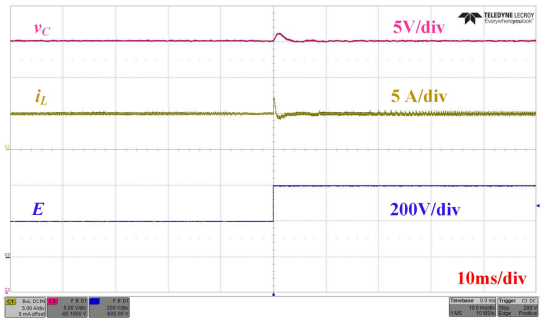

(a)

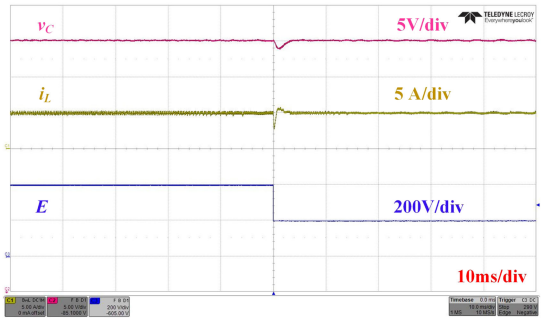

(b)

Fig. 15. Experimental results with input voltage variation.

from 200 to 400 V; Fig. 15(b) shows dynamic response when input voltage steps down from 400 to 200 V. As can be observed, with the input voltage variation, the bus voltage maintains at 100 V with negligible disturbances and the impact on inductor current is also negligible with the transient time around 2 ms.

VI. Conclusion

This article proposes an offset-free MPC for dc/dc buck converter feeding CPLs. The receding horizon optimization problem is formulated with the external and model uncertainties estimated by a HOSMO. Then the optimal control law is derived by solving the integrated optimization problem offline. The obtained composite MPC controller is expressed as a simple linear form with optimally designed parameters. The large signal stability of the proposed controller is ensured by a rigorous stability analysis. The proposed approach has the advantages of optimized dynamics, accurate voltage tracking with strong robustness against external and system uncertainties. The effectiveness of the proposed controller is verified by simulation and experimental studies.

Appendix

A. Higher Order Sliding Mode Observer

For a system

$$\dot{x} = f(x, u; t) + w(t) \tag{A.1}$$

where $w(t)$ is the disturbance.

A HOSMO can be designed as

$$\begin{cases} \dot{z}_0 = v_0 + f(x,u,t), \\ v_0 = -\lambda_0 L_d^{1/(l+1)} \mathrm{sig}^{l/(l+1)}(z_0 - x) + z_1 \\ \dot{z}_1 = v_1, v_1 = -\lambda_1 L_d^{1/l} \mathrm{sig}^{(l-1)/l}(z_1 - v_o) + z_2 \\ \vdots \\ \dot{z}_{l-1} = v_{l-1}, v_{l-1} = -\lambda_{l-1} L_d^{1/2} \mathrm{sig}^{1/2}(z_{l-1} - v_{l-2}) + z_l \\ \dot{z}_l = v_l, v_l = -\lambda_l L_d \mathrm{sig}(z_l - v_{l-1}) \\ \hat{x} = z_0, \hat{w} = z_1, \ldots, \hat{w}^{(l-1)} = z_l \end{cases} \tag{A.2}$$

where λ_i are observer coefficients, L_d is the scaling gain, and $\hat{x}, \hat{w}, \ldots, \hat{w}^{(l-1)}$ are estimates of $z_0, z_1, \ldots, z_l$. Function $\mathrm{sig}^a(\cdot)$ is defined by $\mathrm{sig}^a(\cdot) = \mathrm{sign}(\cdot)|\cdot|^a$ with $\mathrm{sign}(\cdot)$ denoting the standard signum function and a being a constant.

The error system of (A.2) can be derived as

$$\begin{cases} \dot{e}_0 = -\lambda_0 L_d^{1/(l+1)} \mathrm{sig}^{l/(l+1)}(e_0) + e_1 \\ \dot{e}_1 = -\lambda_1 L_d^{1/l} \mathrm{sig}^{(l-1)/l}(e_1 - \dot{e}_o) + e_2 \\ \vdots \\ \dot{e}_{l-1} = -\lambda_{l-1} L_d^{1/2} \mathrm{sig}^{1/2}(e_{l-1} - \dot{e}_{l-2}) + e_l \\ \dot{e}_l \in -\lambda_l L_d \mathrm{sig}(e_l - \dot{e}_{l-1}) + [-L_d, L_d] \end{cases} \tag{A.3}$$

where the estimation errors are defined as $e_0 = z_0 - x, e_1 = z_1 - w, \ldots, e_l = z_l - w^{(l-1)}$.

It follows from [25] that observer error system (A.2) is finite-time stable, that is, there exists a time constant $t_f > t_0$ such that $e_i(t) = 0 (i = 0, 1, \ldots, l)$ (or equivalently $\hat{x} = z_0, \hat{w} = z_1, \ldots, \hat{w}^{(l-1)} = z_l$).

B. Tuning of the Higher Order Sliding Mode Observer

A proper L_d should be selected to ensure fast convergence of the estimation values to real ones. At the current stage, the design of nonlinear control parameters is normally based on trial-and-error manner [24]. Therefore, we tune L_d through trial and error based on the experience from existing works [25], [28].

Fig. 16 shows dynamic performance of system with different values of L_d ($L_d = 10^{12}$, 10^{13}, 10^{14} and 10^{15}). The CPL increases from 500 W to 1 kW at 0.04 s. As can be observed, a larger L_d causes shorter transient period. But a common problem of existing high gain control methods is that a larger gain will cause deterioration of system robustness against the measurement noise. Therefore, we should select a proper value based on the required system dynamics. In this case, L_d is selected at 10^{14} to have dynamics of 2 ms.

C. Lemma 1

Lemma 1 (Schur Decomposition Bound): [29]: The inequality $\exp(At) \le \exp(\alpha(A)t) \sum_{k=0}^{n-1} \|N\|^2/k!$ holds for all $A \in R_{n\times n}$, where $\alpha(A) \in R$ is the maximum real part of eigenvalues of A and $N \in R_{n\times n}$ is the Schur decomposition matrix of A.

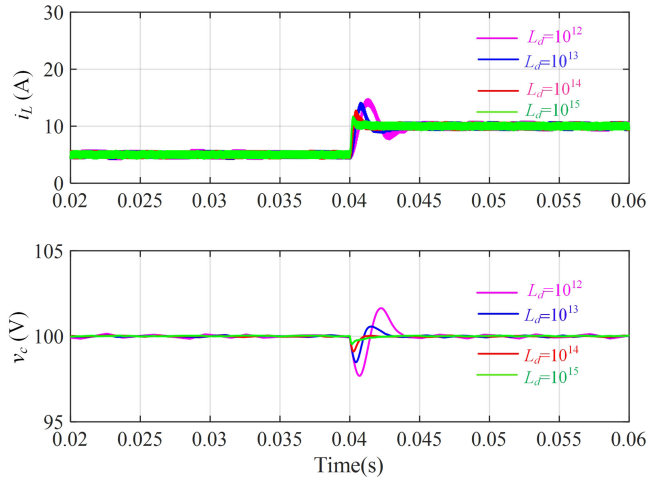

Fig. 16. System dynamic response with different values of L_d in HOSMO.

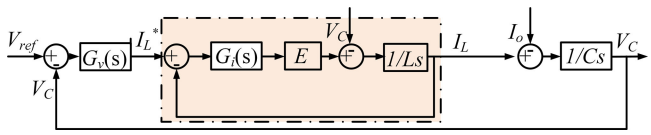

Fig. 17. Control diagram of the double-loop PI controller for the buck converter system.

D. Parameter Design of Double-Loop PI Control

The double-loop PI controller utilized in Fig. 8 is designed by following a standard design guideline recommended by [27], [30]. It is based on the linearized model in frequency domain. By following this guideline, it has an advantage that the parameters are designed given the expected dynamic performance with enough stability margin. Using this method, the load current is treated as a disturbance and we do not need to consider a specific operating power during the design of the PI parameters.

Fig. 17 shows the control diagram for a buck converter with double loop PI controller. G_v and G_i are the PI loops for voltage and current regulation, respectively. Then in accordance with [30], two main considerations for the compensator design have to be made: 1) The dynamic response of current loop should be much slower than the PWM modulator and much faster than that of voltage loop; 2) The stability margin of both current and voltage loops should be regulated sufficiently large to guarantee the overall stable operations.

First, the voltage loop is designed. As the current loop is designed fast enough than voltage loop, the open-loop transfer function of current control, which is shown in the dashed box, can be seen as a gain of 1. Then the voltage control loop is simplified as

$$[(V_{\text{ref}} - V_C)G_v(s) - I_o]\frac{1}{Cs} = V_C. \tag{A.4}$$

The open loop transfer T_{vo} for voltage control can be expressed as

$$T_{vo}(s) = G_v(s)\frac{1}{Cs} \tag{A.5}$$

where the voltage loop PI controller is expressed as

$$G_v(s) = k_{vp} + \frac{k_{vi}}{s}. \tag{A.6}$$

Define ω_v as the control bandwidth of voltage control loop. To ensure enough phase margin, corner frequency of the PI compensator $\frac{k_{vp}}{k_{vi}}$ should be less than ω_v, which can be expressed as

$$\frac{k_{vp}}{k_{vi}} = \eta\omega_v \tag{A.7}$$

where is η a small value between 1/10–1/5 and a smaller η gives a larger phase margin.

To design the voltage controller, the gain of the open-loop voltage transfer function T_{vo} at ω_v should be 1, which results in

$$T_{vo}(j\omega_v) = \left|\frac{k_{vp}(j\omega_v + \eta\omega_v)}{j\omega_v}\frac{1}{Cj\omega_v}\right| = 1. \tag{A.8}$$

As η is much less than 1, it can be neglected in (A.8) and the voltage controller parameters can be calculated as

$$\begin{cases} k_{vp} = \omega_v C \\ k_{vi} = \eta\omega_v^2 C. \end{cases} \tag{A.9}$$

Inner current loop can be designed following the procedure similar to (A.4)–(A.9). The current PI controller parameters are calculated as

$$\begin{cases} k_{ip} = \frac{\omega_i L}{E} \\ k_{ii} = \frac{\eta\omega_i^2 L}{E} \end{cases} \tag{A.10}$$

where ω_i is the control bandwidth of current control loop.

REFERENCES

[1] F. Katiraei, R. Iravani, N. Hatziargyriou, and A. Dimeas, "Microgrids management," *IEEE Power Energy Mag.*, vol. 6, no. 3, pp. 54–65, May/Jun. 2008.
[2] J. Xiao, P. Wang, and L. Setyawan, "Hierarchical control of hybrid energy storage system in dc microgrids," *IEEE Trans. Ind. Electron.*, vol. 62, no. 8, pp. 4915–4924, Aug. 2015.
[3] C. Jin, P. Wang, J. Xiao, Y. Tang, and F. H. Choo, "Implementation of hierarchical control in dc microgrids," *IEEE Trans. Ind. Electron.*, vol. 61, no. 8, pp. 4032–4042, Aug. 2014.
[4] T. Dragičević, X. Lu, J. C. Vasquez, and J. M. Guerrero, "DC microgrids-part i: A review of control strategies and stabilization techniques," *IEEE Trans. Power Electron.*, vol. 31, no. 7, pp. 4876–4891, Jul. 2016.
[5] A. Emadi, A. Khaligh, C. H. Rivetta, and G. A. Williamson, "Constant power loads and negative impedance instability in automotive systems: Definition, modeling, stability, and control of power electronic converters and motor drives," *IEEE Trans. Veh. Technol.*, vol. 55, no. 4, pp. 1112–1125, Jul. 2006.
[6] Q. Xu, P. Wang, J. Chen, C. Wen, and M. Y. Lee, "A module-based approach for stability analysis of complex more-electric aircraft power system," *IEEE Trans. Transp. Electrific.*, vol. 3, no. 4, pp. 901–919, Dec. 2017.
[7] A. Kwasinski and C. N. Onwuchekwa, "Dynamic behavior and stabilization of dc microgrids with instantaneous constant-power loads," *IEEE Trans. Power Electron.*, vol. 26, no. 3, pp. 822–834, Mar. 2011.
[8] A. Riccobono and E. Santi, "Comprehensive review of stability criteria for dc power distribution systems," *IEEE Trans. Ind. Appl.*, vol. 50, no. 5, pp. 3525–3535, Sep./Oct. 2014.
[9] M. Cespedes, L. Xing, and J. Sun, "Constant-power load system stabilization by passive damping," *IEEE Trans. Power Electron.*, vol. 26, no. 7, pp. 1832–1836, Jul. 2011.

[10] X. Zhang, X. Ruan, and Q.-C. Zhong, "Improving the stability of cascaded dc/dc converter systems via shaping the input impedance of the load converter with a parallel or series virtual impedance," *IEEE Trans. Ind. Electron.*, vol. 62, no. 12, pp. 7499–7512, Dec. 2015.
[11] X. Lu, K. Sun, J. M. Guerrero, J. C. Vasquez, L. Huang, and J. Wang, "Stability enhancement based on virtual impedance for dc microgrids with constant power loads," *IEEE Trans. Smart Grid*, vol. 6, no. 6, pp. 2770–2783, Nov. 2015.
[12] X. Zhang and Q.-C. Zhong, "Improved adaptive-series-virtual-impedance control incorporating minimum ripple point tracking for load converters in dc systems," *IEEE Trans. Power Electron.*, vol. 31, no. 12, pp. 8088–8095, Dec. 2016.
[13] C. N. Onwuchekwa and A. Kwasinski, "Analysis of boundary control for buck converters with instantaneous constant-power loads," *IEEE Trans. Power Electron.*, vol. 25, no. 8, pp. 2018–2032, Aug. 2010.
[14] Y. Zhao, W. Qiao, and D. Ha, "A sliding-mode duty-ratio controller for dc/dc buck converters with constant power loads," *IEEE Trans. Ind. Appl.*, vol. 50, no. 2, pp. 1448–1458, Mar./Apr. 2014.
[15] Q. Xu, C. Zhang, C. Wen, and P. Wang, "A novel composite nonlinear controller for stabilization of constant power load in dc microgrid," *IEEE Trans. Smart Grid*, vol. 10, no. 1, pp. 752–761, Jan. 2019.
[16] S. Yousefizadeh, J. D. Bendtsen, N. Vafamand, M. H. Khooban, F. Blaabjerg, and T. Dragičević, "Tracking control for a dc microgrid feeding uncertain loads in more electric aircraft: Adaptive backstepping approach," *IEEE Trans. Ind. Electron.*, vol. 66, no. 7, pp. 5644–5652, Jul. 2019.
[17] M. A. Kardan *et al.*, "Improved stabilization of nonlinear dc microgrids: Cubature Kalman filter approach," *IEEE Trans. Ind. Appl.*, vol. 54, no. 5, pp. 5104–5112, Sep./Oct. 2018.
[18] M. A. Hassan, E.-P. Li, X. Li, T. Li, C. Duan, and S. Chi, "Adaptive passivity-based control of dc– dc buck power converter with constant power load in dc microgrid systems," *IEEE J. Emerg. Sel. Topics Power Electron.*, vol. 7, no. 3, pp. 2029–2040, Sep. 2019.
[19] X. Zhang, B. Wang, U. Manandhar, H. B. Gooi, and G. Foo, "A model predictive current controlled bidirectional three-level dc/dc converter for hybrid energy storage system in dc microgrids," *IEEE Trans. Power Electron.*, vol. 34, no. 5, pp. 4025–4030, May 2019.
[20] T. Dragičević, "Dynamic stabilization of dc microgrids with predictive control of point-of-load converters," *IEEE Trans. Power Electron.*, vol. 33, no. 12, pp. 10872–10884, Dec. 2018.
[21] Z. Ma, X. Zhang, J. Huang, and B. Zhao, "Stability-constraining-dichotomy-solution-based model predictive control to improve the stability of power conversion system in the MEA," *IEEE Trans. Ind. Electron.*, vol. 66, no. 7, pp. 5696–5706, Jul. 2019.
[22] J. Yang, W. X. Zheng, S. Li, B. Wu, and M. Cheng, "Design of a prediction-accuracy-enhanced continuous-time MPC for disturbed systems via a disturbance observer," *IEEE Trans. Ind. Electron.*, vol. 62, no. 9, pp. 5807–5816, Sep. 2015.
[23] C. Zhang, Y. Yan, A. Narayan, and H. Yu, "Practically oriented finite-time control design and implementation: Application to a series elastic actuator," *IEEE Trans. Ind. Electron.*, vol. 65, no. 5, pp. 4166–4176, May 2018.
[24] S. Li, J. Yang, W.-H. Chen, and X. Chen, *Disturbance Observer-Based Control: Methods and Applications*. Boca Raton, FL, USA: CRC Press, 2014.
[25] A. Levant, "Higher-order sliding modes, differentiation and output-feedback control," *Int. J. Control*, vol. 76, no. 9/10, pp. 924–941, 2003.
[26] C.-T. Chen, *Linear System Theory and Design*. London, U.K.: Oxford Univ. Press, 1998.
[27] S. Bacha *et al.*, "Power electronic converters modeling and control," in *Advanced Textbooks in Control and Signal Processing, vol. 454*. London, U.K.: Springer, 2014.
[28] Y. Shtessel, C. Edwards, L. Fridman, and A. Levant, *Sliding Mode Control and Observation*. Berlin, Germany: Springer, 2014.
[29] C. V. Loan, "The sensitivity of the matrix exponential," *J. Numer. Anal.*, vol. 14, no. 6, p. 971–981, 1977.
[30] Q. Xu *et al.*, "A decentralized dynamic power sharing strategy for hybrid energy storage system in autonomous dc microgrid," *IEEE Trans. Ind. Electron.*, vol. 64, no. 7, pp. 5930–5941, Jul. 2017.

Qianwen Xu (S'14–M'18) received the B.Sc. degree from Tianjin University, Tianjin, China, in 2014 and the Ph.D. degree from Nanyang Technological University, Singapore, in 2018, both in electrical engineering.

She has worked as a Research Associate with Hong Kong Polytechnic University, Hong Kong, and a Postdoctoral Research Fellow with Aalborg University, Aalborg, Denmark, in 2018. She is currently a Wallenberg-NTU Presidential Postdoctoral Fellow with Nanyang Technological University, Singapore. Her research interests include control, stability, reliability, and optimization of microgrids and smart grids.

Yunda Yan (S'15–M'18) received the B.Sc. degree in automation and the Ph.D. degree in control theory and control engineering from the School of Automation in Southeast University, Nanjing, China, in 2013 and 2019, respectively. He was a Visiting Student with the Department of Biomedical Engineering, National University of Singapore, Singapore, in 2017, and the Department of Aeronautical and Automotive Engineering, Loughborough University, Loughborough, U.K., in 2018.

His current research interests include the development of predictive control methods, dynamic high-gain control methods, control allocation methods, and disturbance modeling and estimation approaches and their applications in motion/flight control systems.

Chuanlin Zhang (M'14–SM'19) received the B.S. degree in mathematics and the Ph.D. degree in control theory and control engineering from the School of Automation, Southeast University, Nanjing, China, in 2008 and 2014, respectively. He was a Visiting Ph.D. Student with the Department of Electrical and Computer Engineering, University of Texas at San Antonio, TX, USA, from 2011 to 2012.

He was a Visiting Scholar with the Energy Research Institute, Nanyang Technological University, Singapore, from 2016 to 2017, and with Advanced Robotics Center, National University of Singapore, Singapore, from 2017 to 2018. Since 2014, he has been with the College of Automation Engineering, Shanghai University of Electric Power, Shanghai, China, where he is currently a Professor. He is the Principal Investigator of several research projects, including the Eastern Scholar Program at Shanghai, Leading Talent Program of Shanghai Science and Technology Commission, Chenguang Program by the Shanghai Municipal Education Commission, etc. His research interests include nonlinear system control theory and applications for power systems.

Tomislav Dragicevic (S'09–M'13–SM'17) received the M.Sc. and the industrial Ph.D. degrees in electrical engineering from the Faculty of Electrical Engineering, Zagreb, Croatia, in 2009 and 2013, respectively.

From 2013 until 2016 he has been a Postdoctoral Research Associate with Aalborg University, Aalborg, Denmark. From March 2016 he is an Associate Professor at Aalborg University, where he leads an Advanced Control Lab. He was a Guest Professor at Nottingham University, U.K., during spring/summer of 2018. He has authored and coauthored more than 170 technical papers (more than 70 of them are published in international journals, mostly IEEE transactions) in his domain of interest, eight book chapters, and a book in the field. His research interests include design and control of microgrids and application of advanced modeling and control concepts to power electronic systems.

Dr. Dragievi was the recipient of the Konar Prize for the best industrial Ph.D. thesis in Croatia, and the Robert Mayer Energy Conservation Award. He serves as the Associate Editor in the IEEE TRANSACTIONS ON INDUSTRIAL ELECTRONICS, the IEEE EMERGING AND SELECTED TOPICS IN POWER ELECTRONICS, and the IEEE INDUSTRIAL ELECTRONICS MAGAZINE.

Frede Blaabjerg (S'86–M'88–SM'97–F'03) received the Ph.D. degree in electrical engineering from Aalborg University, Aalborg, Denmark, in 1995.

He was with ABB-Scandia, Randers, Denmark, from 1987 to 1988. He became an Assistant Professor in 1992, an Associate Professor in 1996, and a Full Professor of Power Electronics and Drives in 1998. From 2017 he became a Villum Investigator. He is *honoris causa* at University Politehnica Timisoara (UPT), Timisoara, Romania and Tallinn Technical University (TTU) in Tallinn, Estonia. He has authored and coauthored more than 600 journal papers in the fields of power electronics and its applications. He is the Co-Author of four monographs and editor of ten books in power electronics and its applications. His current research interests include power electronics and its applications such as in wind turbines, PV systems, reliability, harmonics, and adjustable speed drives.

Dr. Blaabjerg was recipient of 31 IEEE Prize Paper Awards, the IEEE PELS Distinguished Service Award in 2009, the EPE-PEMC Council Award in 2010, the IEEE William E. Newell Power Electronics Award 2014, the Villum Kann Rasmussen Research Award 2014, and the Global Energy Prize in 2019. He was the Editor-in-Chief of the IEEE TRANSACTIONS ON POWER ELECTRONICS from 2006 to 2012. He has been Distinguished Lecturer for the IEEE Power Electronics Society from 2005 to 2007 and for the IEEE Industry Applications Society from 2010 to 2011 as well as 2017 to 2018. He serves a the President of IEEE Power Electronics Society. He is the Vice-President of the Danish Academy of Technical Sciences. He is nominated in 2014–2018 by Thomson Reuters to be between the 250 most cited researchers in engineering in the world.